Journal of Catalysis **192,** 64–76 (2000)
doi:10.1006/jcat.2000.2839, available online at http://www.idealibrary.com on IDEAL®

Adsorptive and Catalytic Properties of Alumina-Supported Pd–Mo Catalysts

M. A. S. Baldanza,* L. F. de Mello,* A. Vannice,† F. B. Noronha,*,[1] and M. Schmal*,[2]

*NUCAT-PEQ-COPPE, Universidade Federal do Rio de Janeiro, Ilha do Fundão, C.P. 68502, CEP 21941, Rio de Janeiro, Brazil; and †Department of Chemical Engineering, Pennsylvania State University, University Park, Pennsylvania 16802

Received August 26, 1999; revised January 24, 2000; accepted January 28, 2000

The adsorption properties of ethanol, CO, and NO on Pd, Mo, and Pd–20Mo/Al_2O_3 catalysts were studied using TPD and IR techniques as well as the reactions of NO + CO and ethanol + NO. The presence of Pd favored decomposition and dehydrogenation of ethanol, while Mo presented activity for oxidative dehydrogenation. The Pd–Mo catalyst showed better formation of N_2 on TPD of NO, probably due to the NO adsorption on partially reduced molybdenum oxide. DRIFT results for the NO + CO reaction on the Pd–20Mo catalyst exhibited bands which correspond to nitrate or nitrous complexes and hydroxyl groups besides NCO species. MoO_3 addition to a Pd/Al_2O_3 catalyst favored the formation of acetaldehyde at lower temperatures. A redox mechanism was proposed to explain the molybdenum promotional effect on Pd in the CO + NO reaction, evidencing Mo as promoter when the reducible oxide reacts with NO. However, molybdenum oxide does not promote the ethanol + NO reaction and this may be due to different reaction mechanisms.

Key Words: **palladium; molybdenum; TPD and reactions; NO; CO; ethanol; DRIFT.**

INTRODUCTION

It is known that emission control of conventional pollutants may be partially achieved by using oxygenated organic compounds as fuel or fuel additives. Recently, alcohols and ethers have been used together with gasoline as fuel for automotive vehicles. In this case, carbon monoxide emissions by ethanol-fueled vehicles are substantially reduced. However, the use of ethanol increased the direct emissions of unburned ethanol and aldehydes (acetaldehyde and formaldehyde) in the exhaust gases (1). These products have potential carcinogenic effects and react forming photochemically active radicals and toxic peroxyacetyl nitrate (2). Therefore, such systems need better emission control by using adequate catalytic converters.

Pd–Mo/Al_2O_3 catalysts have been used to control the exhaust emissions of ethanol-fueled Brazilian vehicles (3). It has been reported that the addition of MoO_3 to Pd/Al_2O_3 catalysts improved the NO activity with high selectivity to N_2 in the presence of a small excess of oxygen (4–6). According to Ghandi *et al.* (4), the high selectivity for NO reduction is due to Pd–Mo interactions. On the basis of TPR and IR analysis, they ascribed these results to the presence of a surface Pt^o–Mo^{4+} complex that had activity and selectivity behavior similar to that observed on rhodium catalysts. However, it is not clear how the molybdenum oxide affects the adsorptive properties of the noble metal in order to explain the catalytic behavior of these systems. In a previous work (7), Pd–Mo/Al_2O_3 catalysts were studied for the CO + NO reaction. An 8% Mo loading was used and a high selectivity for N_2 formation was observed and explained through a redox mechanism, where the presence of partially reduced molybdenum oxide in contact with palladium particles was necessary. Furthermore, another work studied the effect of the precursor salts on the CO and NO adsorption properties of Pd–Mo/Al_2O_3 catalysts (8).

Nevertheless, no work has been done to study the effect of oxygenated organic compounds on the adsorption and catalytic properties of Pd–Mo/Al_2O_3 catalysts regarding the CO + NO reaction. Some work has been done focusing on the complete oxidation of alcohols and aldehydes on several noble metal and metal oxide catalysts (9–12). However, most of the work has been carried out to measure conversion and selectivity as a function of temperature. Fundamental research was presented by Cordi and Falconer (13) on the oxidation of ethanol and acetaldehydes on alumina-supported palladium catalysts using temperature-programmed desorption (TPD) and oxidation (TPO). Idriss *et al.* (14) studied the reactions of acetaldehyde on the surface of CeO_2-supported palladium catalysts also using TPD and IR analyses.

The present paper focuses attention on the adsorption capacity and surface reactivity in the CO + NO and ethanol + NO reactions on Pd/Al_2O_3 and Pd–MoO_3/Al_2O_3 catalysts with a high Mo loading (20%), as determined by DRIFTS, TPD, FTIR, and reactivity tests.

[1] Present address: Instituto Nacional de Tecnologia-INT, Av. Venezuela 82, CEP 20081-310, Rio de Janeiro, Brazil. Fax: (55-21) 2636552. E-mail: bellot@int.gov.br.

[2] To whom correspondence should be addressed. Fax: (55-21) 2906626. E-mail: schmal@peq.coppe.ufrj.br.

0021-9517/00 $35.00

EXPERIMENTAL

Catalyst Preparation

A 20% Mo/Al_2O_3 catalyst was prepared by wet impregnation of Al_2O_3 (Engelhard; BET area = 189 m^2/g) with an aqueous solution of $(NH_4)_6Mo_7O_{24} \cdot 4H_2O$. The sample was dried at 383 K for 22 h and calcined under flowing air at 773 K for 2 h. Pd/Al_2O_3 and $Pd–Mo/Al_2O_3$ samples were obtained by wet impregnation of Al_2O_3 and Mo/Al_2O_3, respectively, with a solution of $Pd(NO_3)_2$ (Aldrich). Then the samples were dried at 373 K and calcined under flowing air at 773 K for 2 h. The prepared catalysts, their nomenclature, and their composition are presented in Table 1.

Catalyst Characterization

H_2 and CO chemisorption. H_2 and CO uptakes were measured using ASAP 2000C equipment (Micromeritics). Before the reduction, the catalysts were dehydrated at 423 K for 0.5 h. Then the catalysts were reduced at 773 K (5 K/min.) in flowing H_2 (30 cm^3/min.). Following reduction, the samples were evacuated for 1 h at reduction temperature and cooled to adsorption temperature under vacuum. Irreversible uptakes were determined from dual isotherms measured for hydrogen (at 343 K) and carbon monoxide (at 298 K).

Temperature-programmed desorption (TPD). TPD of adsorbed CO, NO, or ethanol was carried out in a microreactor coupled to a quadrupole mass spectrometer (Prisma, Balzers). A Quadstar analytical system was used for selecting and recording different signal intensities of masses as a function of the temperature. The procedure was similar for all experiments. First, the catalyst sample was purged under helium flow (50 cm^3/min.) from room temperature up to 823 K at a heating rate of 10 K/min. The sample was then cooled and reduced under flowing H_2 (30 cm^3/min) up to 773 K for 2 h. Following reduction, the system was outgased with helium flow at the reduction temperature for 30 min and cooled to room temperature. The adsorption of CO, NO, or ethanol was performed by introducing pulses of 5% CO in helium (AGA >99%) or 1% NO in helium (AGA S.A. >99%) until saturation. The ethanol adsorption was made using pulses of an ethanol + He mixture, obtained by passing He through a saturator containing ethanol at room temperature. After adsorption, the catalyst sample was heated at 20 K/min to 823 K in flowing helium (50 cm^3/min).

The mass spectrometer was calibrated against helium mixtures containing specified concentrations of CO, NO, N_2O, ethanol, or acetaldehyde and pure CO_2, H_2, N_2, ethylene, and Ar. The fragmentation pattern of each individual product was determined experimentally in the mass spectrometer. The corresponding values obtained are presented in Table 2. The correction procedure to determine the distribution of the desorbed products was made as follows. From the most intense fragment of each product (such as $m/e = 44$ for CO_2) it was possible to determine the corresponding amounts of its secondary fragments (in this example, $m/e = 28$), taking into account the intensity ratios of the mass fragments. After subtraction of the contribution from carbon dioxide, the remaining signal of $m/e = 28$ was assigned to carbon monoxide. The same procedure was adopted for the desorption spectra of the nitrogen-containing compounds.

Infrared spectroscopy of adsorbed ethanol. Ethanol adsorption was monitored using a Fourier transform infrared spectrometer (Perkin Elmer 2000). The catalysts were reduced with H_2 at 773 K for 1 h. After evacuation at the reduction temperature for 1 h and cooling down to room temperature, ethanol uptake was allowed until saturation at 298 K, followed by FTIR measurements under vacuum at 298, 373, 423, 473, 523, and 573 K.

DRIFTS analysis. The DRIFTS measurements were obtained with an upgraded Sirius 100 FTIR system (Matheson Instruments) using a DRIFTS cell (HVC-DRP, Harrick Scientific). The system is described elsewhere in detail (15). The sample holder had approximately 50 mg of Al_2O_3 with 30 mg of the catalyst placed on top for DRIFTS studies. The sample was prereduced by flowing a 1% H_2/He mixture. Spectra were then taken following the three sequential treatments: (1) a mixture of 0.6% NO in He was passed for

TABLE 1

Catalyst Composition

Catalyst	Pd (wt%)	Mo (wt%)
Pd/Al_2O_3	0.97	—
$20Mo/Al_2O_3$	—	19.9
$Pd–20Mo/Al_2O_3$	0.91	19.31

TABLE 2

Major Fragments of Products Desorbed during CO, NO, or Ethanol TPD and Intensity Ratios of Mass Fragments

Products	Major fragments	Intensity ratios for mass fragments
CO	**28**	—
CO_2	**44**, 28	44/28 = 9.96
N_2	**28**	—
NO	**30**	—
N_2O	**44**, 30, 28	44/28 = 7.80
		44/30 = 2.94
C_2H_5OH	**31**, 45, 27, 29	31/29 = 1.30
		31/27 = 2.45
C_2H_4O	**29**, 44	29/44 = 2.20
C_2H_4	**28**, 27	28/27 = 1.36

30 min after purging with Ar; (2) 1.3% CO in He was flowed after purging with Ar; and finally (3) a mixture of 0.6% NO + 1.3% CO in He was flowed after an Ar purge. The temperature was changed during the experiment and the spectra were obtained after exposure for 30 min. The sample interferograms consisted of 1000 signal scans obtained by using a postamplifier gain of 4, an iris setting of 50, and resolution of 4 cm^{-1}, as described elsewhere (15). Each interferogram was Fourier transformed to its frequency component spectrum. The ratio of this spectrum with respect to its reference allowed the determination of the transmittance spectrum from which the absorbance spectrum was obtained. Comparative spectra were obtained after adsorption and reaction at programmed multistep temperatures. The alumina support was used as the reference at each temperature.

Catalytic activity. The catalytic experiments were performed in a glass microreactor at atmospheric pressure. Catalysts (ca. 100 mg for the NO + CO reaction and ca. 140 mg for the NO + ethanol reaction) were pretreated in flowing helium (50 ml/min) at 823 K for 0.5 h and then reduced with pure H_2 at 773 K for 1 h. Two feed mixtures were used for the NO + CO reaction: a reducing mixture consisting of 1.0% CO/0.6% NO and an oxidizing mixture consisting of 0.5% CO/0.7% NO, balanced with He at a flow rate of 150 ml/min (space velocity = 70,000 h^{-1}). The feed mixtures for the NO + ethanol reaction consisted of a reducing mixture with 0.2% ethanol/0.3% NO and an oxidizing mixture with 0.1% ethanol/0.7% NO in He at a flow rate of 250 ml/min (space velocity = 82,500 h^{-1}). The effluent was analyzed by gas chromatography (Chrompack with TCD detector, Chromosorb 102 column and cryogen).

RESULTS

H_2 and CO Chemisorption

Table 3 shows the H_2 and CO uptake for the chemisorption measurements on Pd/Al_2O_3, $Pd–20Mo/Al_2O_3$, and $20Mo/Al_2O_3$ catalysts. The catalysts containing Mo showed a much lower H_2 uptake than the Pd/Al_2O_3 catalyst. However, CO chemisorption was greater on the Mo-containing catalysts.

TABLE 3

H_2 and CO Chemisorption

Catalyst	H_2 uptake (μmol/g cat)	CO uptake (μmol/g cat)	CO/H_2
Pd/Al_2O_3	6.640	29.74	4.5
$20Mo/Al_2O_3$	0.399	45.67	115
$Pd–20Mo/Al_2O_3$	0.970	82.43	85.0

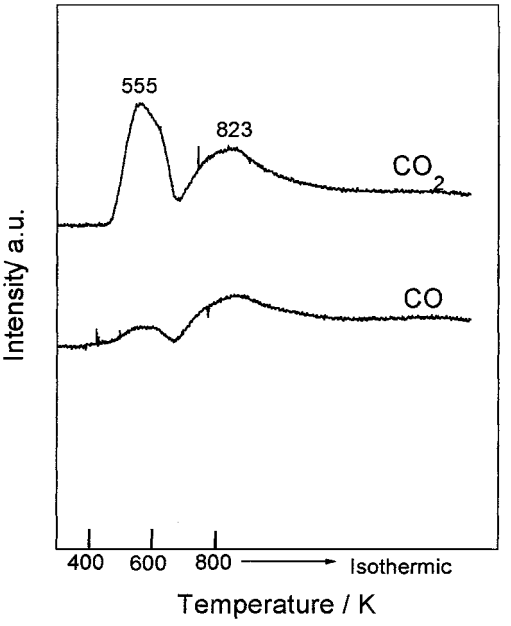

FIG. 1. TPD spectra of CO adsorbed on Pd/Al_2O_3.

CO, NO, and Ethanol Temperature-Programmed Desorption (TPD)

Figures 1, 2, and 3 display the respective TPD profiles after CO adsorption on Pd/Al_2O_3, $20Mo/Al_2O_3$, and $Pd–20Mo/Al_2O_3$ catalysts. In the Pd/Al_2O_3 spectrum, two peaks for the CO desorption were detected at 555 and 823 K with simultaneous formation of CO_2. The spectra

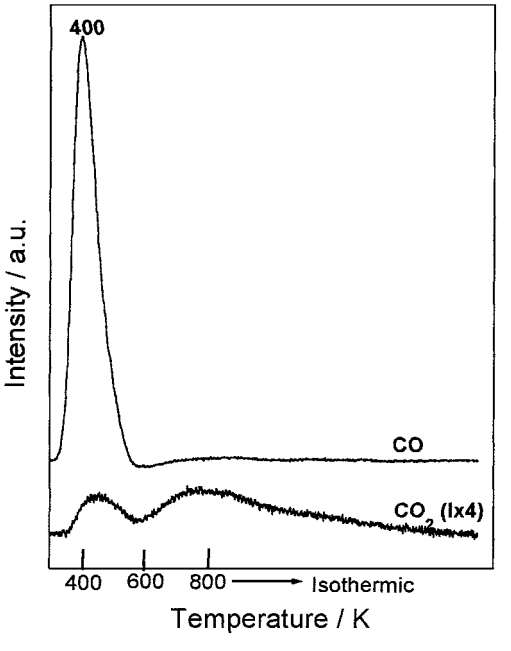

FIG. 2. TPD spectra of CO adsorbed on $20Mo/Al_2O_3$.

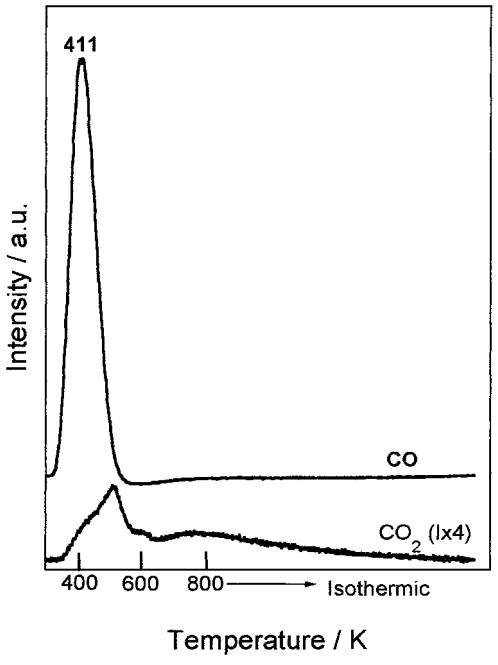

FIG. 3. TPD spectra of CO adsorbed on Pd–20Mo/Al_2O_3.

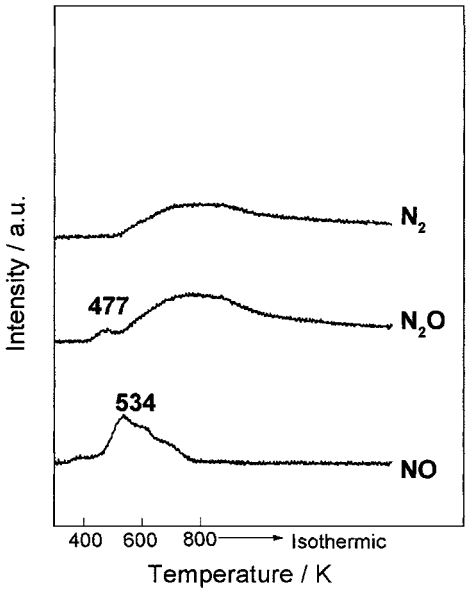

FIG. 4. TPD spectra of NO adsorbed on Pd/Al_2O_3.

for 20Mo/Al_2O_3 and Pd–20Mo/Al_2O_3 showed only one peak for CO desorption around 400 K with little formation of CO_2. The CO desorption increased in the presence of molybdenum as shown from the yield of CO desorption (Table 4).

The respective TPD spectra after NO adsorption on Pd/Al_2O_3, 20Mo/Al_2O_3, and Pd–20Mo/Al_2O_3 catalysts are shown in Figs. 4, 5, and 6. NO, N_2O, and N_2 were the nitrogen-containing products detected during TPD. The Pd/Al_2O_3 catalyst (Fig. 4) presented an NO desorption peak at 534 K and a shoulder around 650 K. The N_2 spectrum exhibited a broad peak around 780 K, and the N_2O curve showed a small peak at 477 K and a broad peak around 780 K. Practically no NO desorption was observed on the Mo-containing catalysts (Table 4). However, two peaks were observed on the N_2 and N_2O profiles of the 20Mo/Al_2O_3 catalyst (Fig. 5), one around 473 K and another one around 795 K. On the Pd–20Mo/Al_2O_3 catalyst, N_2 desorption was observed at 560 and 778 K, with a small shoulder at 475 K (Fig. 6). Nevertheless, it is evident that the presence of MoO_3 decreased NO desorption and promoted the formation of N_2.

Ethanol and ethylene were the main desorption products in the TPD of adsorbed ethanol on alumina (Fig. 7). Ethanol desorbed at two different peaks (395 and 500 K) with a great formation of ethylene around 550 K. No dehydrogenation to acetaldehyde was detected.

The Pd/Al_2O_3 catalyst exhibited a large decrease in ethylene production and the appearance of CO, CH_4, and H_2 formation at 495 K, due to the decomposition of ethanol on Pd (Fig. 8). Moreover, ethanol underwent dehydrogenation to form acetaldehyde at 530 K. A further desorption of CO, H_2, and CO_2 was observed at higher temperatures (above 723 K).

The TPD profiles of ethanol for 20Mo and Pd–20Mo catalysts were very similar (Figs. 9 and 10). Both showed a further decrease in the formation of ethylene and the presence of two other peaks corresponding to acetaldehyde around 473 and 520 K, as well as the desorption of CO, CO_2, and H_2 at higher temperatures. It is important to stress that ethanol decomposition on molybdenum-based catalysts was less important than that on Pd/Al_2O_3.

TABLE 4

Yield (Carbon or Nitrogen Basis) of Products Desorbed during TPD of CO or NO

	Yield (%)		Amount desorbed (μmol/g cat)		Yield (%)		
Catalyst	CO	CO_2	$CO + CO_2$	$NO + N_2O + N_2$	NO	N_2O	N_2
Pd/Al_2O_3	28	72	10	27	42	15	43
20Mo/Al_2O_3	82	18	35	18	0	23	77
Pd–20MoAl_2O_3	83	17	51	52	0	15	85

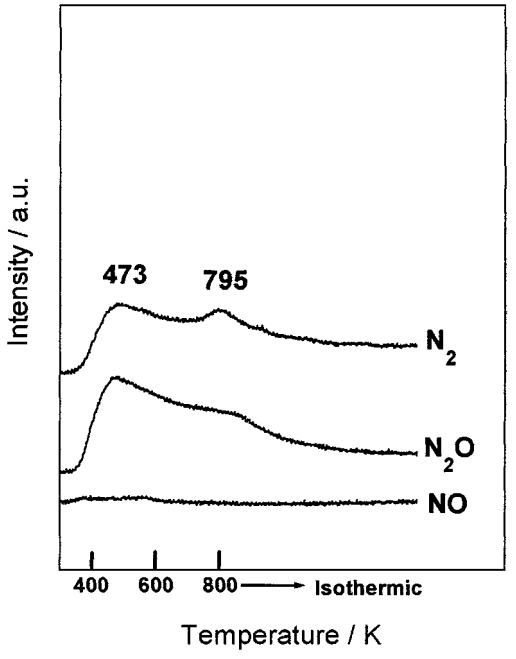

FIG. 5. TPD spectra of NO adsorbed on 20Mo/Al_2O_3.

Infrared Spectroscopy of Adsorbed Ethanol

The IR analysis of ethanol adsorption on the support (Fig. 11) showed characteristic bands of ethoxy species at 1075, 1120, 1168, 1389, and 1447 cm^{-1}. Greenler (16) observed similar bands for the adsorption of ethanol on alumina. Bands at 1585 and 1463 cm^{-1} were attributed to the asymmetric and symmetric stretching of acetate species,

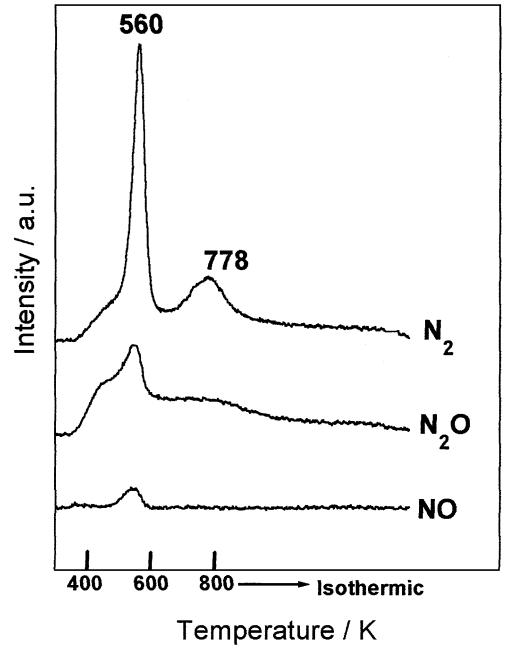

FIG. 6. TPD spectra of NO adsorbed on Pd–20Mo/Al_2O_3.

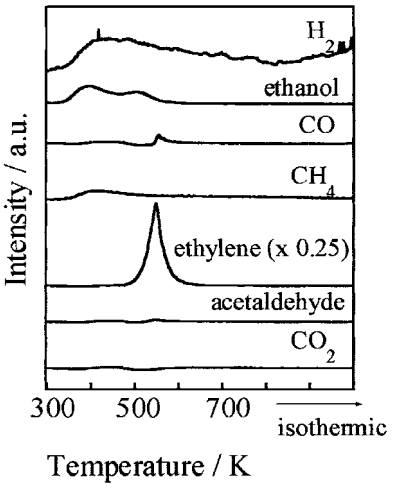

FIG. 7. TPD spectra of ethanol adsorbed on Al_2O_3.

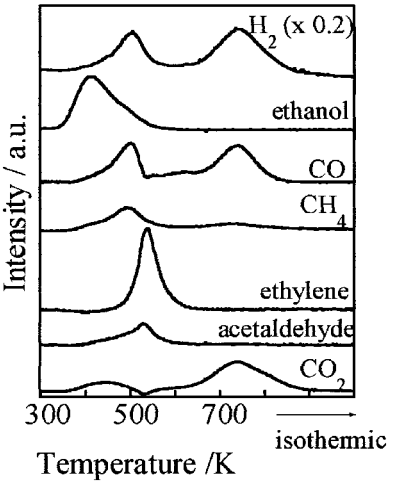

FIG. 8. TPD spectra of ethanol adsorbed on Pd/Al_2O_3.

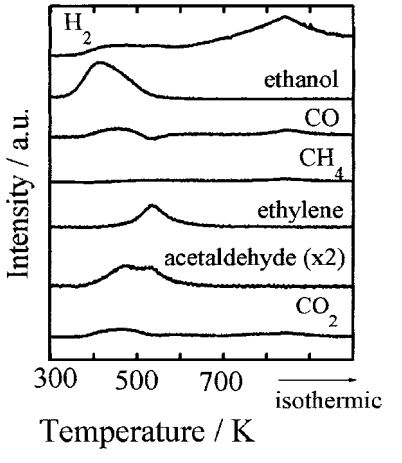

FIG. 9. TPD spectra of ethanol adsorbed on 20Mo/Al_2O_3.

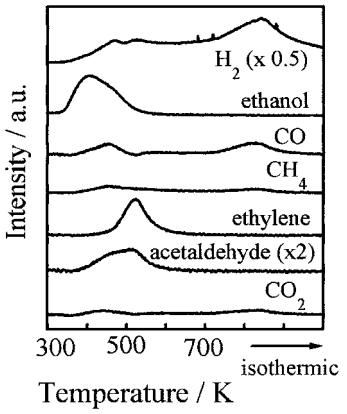

FIG. 10. TPD spectra of ethanol adsorbed on Pd–20Mo/Al_2O_3.

respectively (16). After heating of the sample, the band intensities related to ethoxy species decreased, while those related to acetate species were not modified. The IR spectra of adsorbed ethanol on Pd/Al_2O_3 (Fig. 12) showed, initially, the same bands for ethoxy species as those observed on alumina. However, the band intensities of the ethoxy species decreased, whereas the band intensity related to acetate species increased as the temperature was raised.

For the catalysts containing Mo, it was impossible to obtain FTIR data because there was no transmittance through the reduced samples.

DRIFTS Analysis

Figure 13 displays spectra after NO adsorption on 20% Mo/Al_2O_3 in the oxide form (spectra c and d) and then after

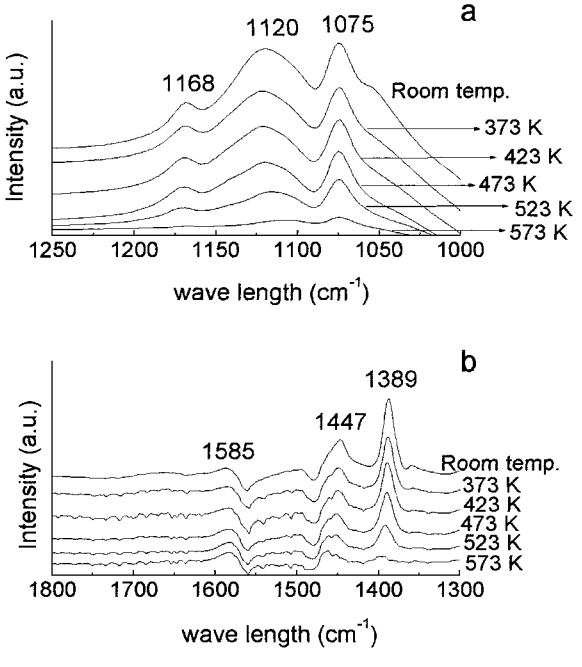

FIG. 11. IR spectra of adsorbed ethanol on Al_2O_3.

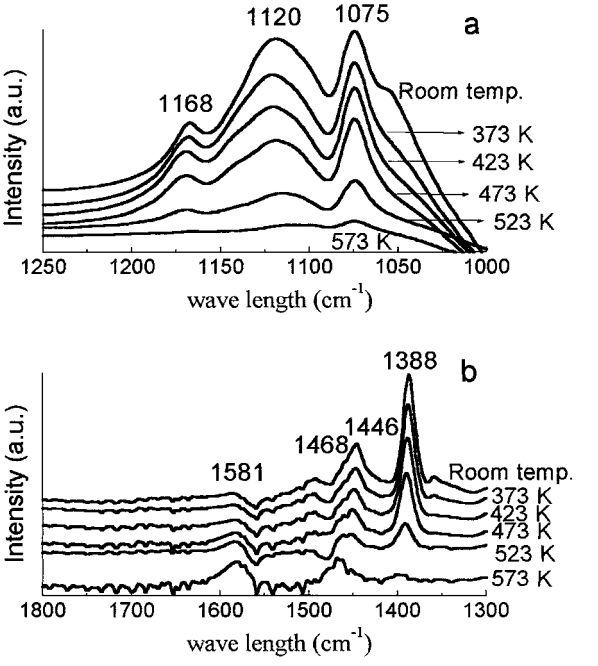

FIG. 12. IR spectra of adsorbed ethanol on Pd/Al_2O_3.

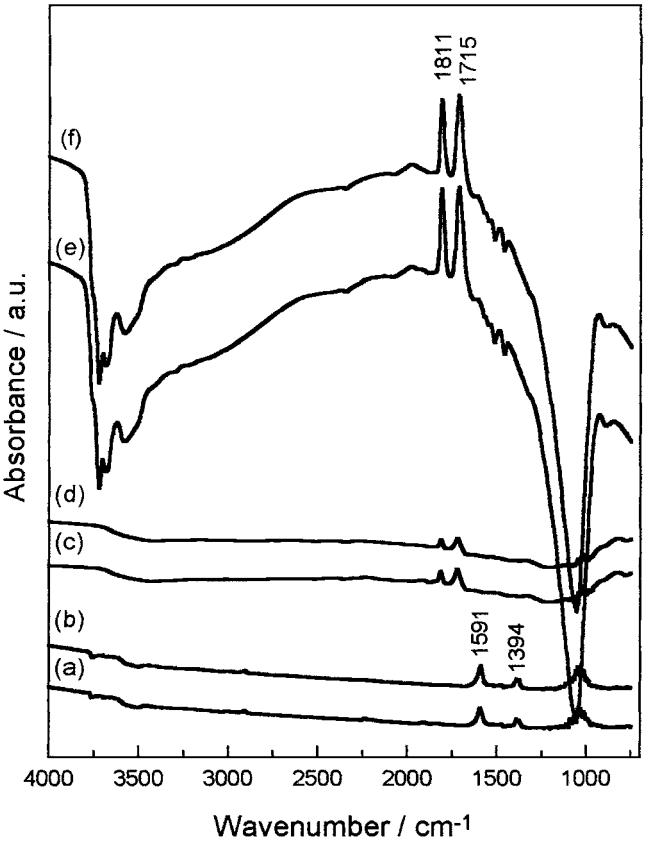

FIG. 13. Drift spectra of (a) NO on Al_2O_3, (b) Al_2O_3 after purging with Ar, (c) NO on 20Mo/Al_2O_3, (d) 20Mo/Al_2O_3 after purging with Ar, (e) NO on reduced 20Mo/Al_2O_3, and (f) reduced 20Mo/Al_2O_3 after purging with Ar.

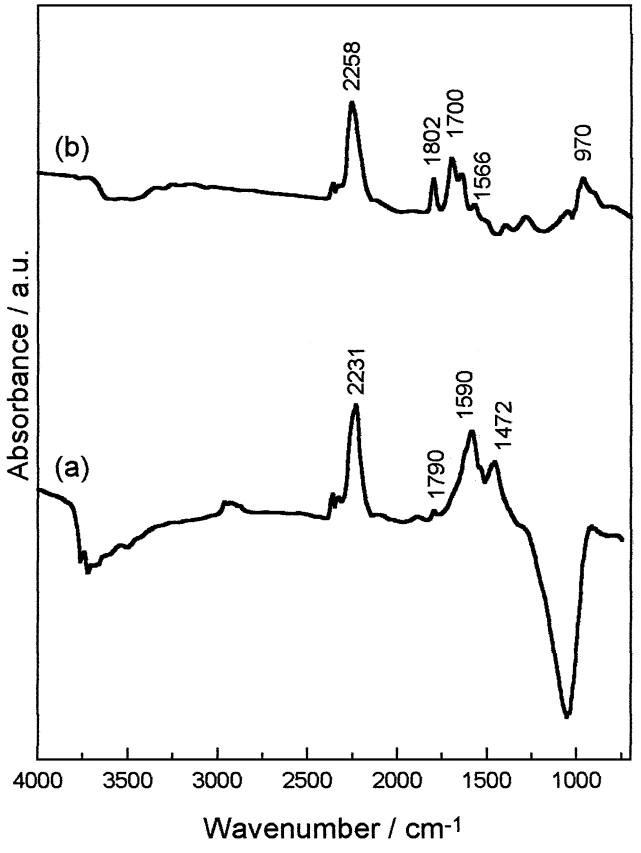

FIG. 14. Drift spectra of NO + CO on (a) Pd/Al_2O_3 and (b) Pd–$20Mo/Al_2O_3$.

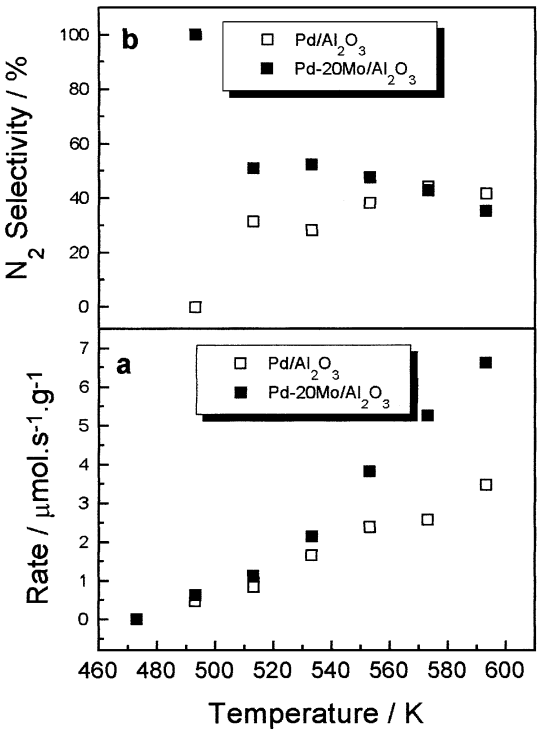

FIG. 15. Behavior of the NO + CO reaction with temperature under reducing conditions over Pd/Al_2O_3 and Pd–$20Mo/Al_2O_3$ catalysts: (a) rate of NO conversion and (b) N_2 selectivity.

reduction in an H_2/He mixture at 773 K (spectra e and f). A sample of Al_2O_3 was investigated as reference (spectra a and b). It was noteworthy that the 20% Mo/Al_2O_3 catalyst showed two bands at 1811 and 1715 cm^{-1}, which strongly increased after reduction.

Figure 14 compares the results after exposure of Pd/Al_2O_3 and Pd–$20Mo/Al_2O_3$ catalysts to NO + CO at 573 K in the DRIFTS cell. The Pd/Al_2O_3 sample exhibited bands at 1472, 1590, and 2231 cm^{-1} (Fig. 14a), while the Pd–$20Mo/Al_2O_3$ catalyst, beside these bands, presented new bands at 1700 and 1802 cm^{-1} (Fig. 14b). The band at 2258 cm^{-1} corresponds to the same band at 2231 cm^{-1} but shifted, which represents the presence of adsorbed NCO species.

Catalytic Activity

Figure 15 displays NO conversion and selectivity as a function of temperature for Pd/Al_2O_3 and Pd–$20Mo/Al_2O_3$ for the NO + CO reaction in a reducing atmosphere (1% CO/0.6% NO). The reaction rate of Pd–$20Mo/Al_2O_3$ between 520 and 600 K was higher than that over Pd/Al_2O_3. The selectivity toward N_2 for Pd/Al_2O_3 and Pd–$20Mo/Al_2O_3$ catalysts is shown in Table 5 for a 10% NO conversion. It is important to notice that for higher conversions, the selectivity for N_2 changed significantly, as shown in Fig. 15. The selectivity is almost the same on both catalysts above 570 K.

Figure 16 shows the NO conversion and selectivity profile for both catalysts for the NO + CO reaction in an oxidizing atmosphere (0.5% CO/0.7% NO). In this case, the activity for the Pd/Al_2O_3 catalyst was higher than that for the Pd–$20Mo/Al_2O_3$ catalyst. However, the selectivity of both catalysts did not vary significantly when compared to the values obtained for the reducing condition (Fig. 15).

Tables 6 and 7 show the activity measurements and selectivity data for the NO + ethanol reaction in a reducing and oxidizing atmosphere, respectively. For the Pd/Al_2O_3

TABLE 5

NO Conversion and Selectivity toward N_2 in NO + CO Reaction at 493 K

Catalyst	CO + NO, Reduction conditions		CO + NO, Oxidation conditions	
	NO conv. (%)	N_2 select. (%)	NO conv. (%)	N_2 select. (%)
Pd/Al_2O_3	8[a]	0	10[a]	0
Pd–$20MoAl_2O_3$	9[a]	100	8[b]	43

[a] NO conversion at 493 K.
[b] NO conversion at 513 K.

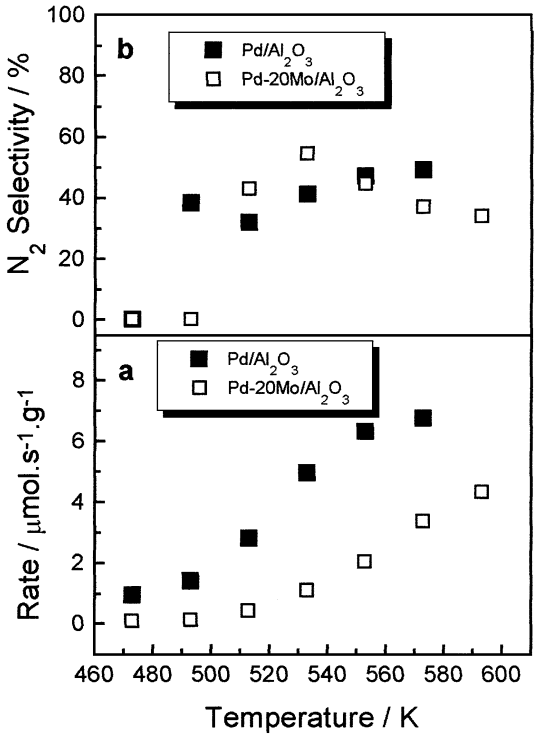

FIG. 16. Behavior of the NO + CO reaction with temperature under oxidizing conditions over Pd/Al_2O_3 and $Pd–20Mo/Al_2O_3$ catalysts: (a) rate of NO conversion and (b) N_2 selectivity.

catalyst, the change from a reducing to an oxidizing atmosphere had no significant influence in the NO conversion and N_2 selectivity.. On the other hand, the ethanol conversion and the ethylene selectivity increased whereas the CO formation decreased. Regardless of the reaction condition, the formation of acetaldehyde on the Pd/Al_2O_3 catalyst was not observed. Ethylene was the main product at low temperature. The increase of the temperature led to a reduction of ethylene selectivity and an increase of CO and CO_2 formation. However, for the $Pd–20Mo/Al_2O_3$ catalyst, the NO conversion decreased significantly for the oxidizing condition. Nevertheless, the selectivity for N_2 formation showed no significant changes. Furthermore, the $Pd–20Mo/Al_2O_3$ catalyst presented a greater formation of acetaldehyde and no production of ethylene under both reaction conditions.

It is important to stress that the $20Mo/Al_2O_3$ catalyst did not exhibit any activity for the reduction of NO on either reaction in the temperature range studied. However, for the NO + ethanol reaction, ethanol was dehydrogenated to form acetaldehyde.

DISCUSSION

CO Adsorption

The carbon monoxide desorption curves for the Pd/Al_2O_3 catalyst, shown in Fig. 1, are in good agreement with those reported previously by Rieck and Bell for Pd/SiO_2 (17–19). Thus, the two peaks at 555 and 823 K observed with the Pd/Al_2O_3 catalyst correspond to the desorption of linear and bridged-bonded CO on Pd, respectively. In addition, two CO_2 peaks were observed at 555 and 823 K. However, since no H_2 evolved with CO_2 at 555 K, the CO_2 formation was attributed to the disproportionation of CO on palladium. Schmal *et al.* (7) demonstrated the presence of carbonaceous species on the palladium surface by performing a TPO analysis after the TPD of CO. The formation of CO_2 during TPO confirmed the carbon deposition on Pd as the result of the Bouduart reaction. On the other hand, in addition to CO_2, small amounts of H_2 and H_2O were detected in the desorbing gas around 823 K. This indicates that the water–gas shift reaction occurred between adsorbed CO and hydroxyl groups on the support in this temperature range (Eqs. 1 and 2) (20).

$$CO + 2OH \rightarrow CO_2 + H_2O \quad [1]$$

$$CO + H_2O \rightarrow CO_2 + H_2. \quad [2]$$

TABLE 6

NO Conversion for the NO + Ethanol Reaction under Reducing Conditions

Catalyst	Temp. (K)	NO conv. (%)	N_2 select. (%)	Ethanol conv. (%)	Selectivity of carbon species[a] (%)			
					CO	CO_2	acetald.	ethyl.
Pd/Al_2O_3	523	0	—	—	—	—	—	
	553	20	72	78	5	33	0	62
	573	29	62	79	13	45	0	42
	593	49	66	85	11	44	0	45
$Pd–20Mo/Al_2O_3$	523	0	—	—	—	—	—	—
	553	0	—	51	0	56	44	0
	573	13	63	60	7	56	37	0
	593	45	67	71	11	51	26	16

[a] acetald. = acetaldehyde; ethyl. = ethylene.

TABLE 7

NO Conversion for the NO + Ethanol Reaction under Oxidizing Conditions

Catalyst	Temp. (K)	NO conv. (%)	N_2 select. (%)	Ethanol conv. (%)	Selectivity of carbon species[a] (%)			
					CO	CO_2	acetald.	ethyl.
Pd/Al_2O_3	523	3	67	69	0	5	0	95
	553	11	73	83	16	43	0	41
	573	30	61	86	6	71	0	23
	593	52	52	100	5	89	0	6
$Pd–20Mo/Al_2O_3$	523	0	—	—	—	—	—	—
	553	0	—	—	—	—	—	—
	573	2	61	76	0	35	65	0
	593	14	59	90	10	90	0	0

[a] acetald. = acetaldehyde; ethyl. = ethylene.

The TPD profile after adsorption of CO on the $20Mo/Al_2O_3$ catalyst showed only one peak around 400 K. Recently, IR analysis revealed the CO adsorption on partially reduced molybdenum oxide (8). Also, TPR measurements up to 773 K showed that molybdenum oxide is partially reduced to Mo^{4+}. Therefore, the single CO desorption peak could be attributed to the adsorption of CO on partially reduced molybdenum oxide. However, only a very small amount of CO_2 was formed and no H_2 or water was observed. This shows that although partially reduced molybdenum oxide adsorbs a reasonable amount of CO (Table 4), it is not very active for the disproportionation reaction. Also, the water–gas shift reaction did not occur, presumably because the high Mo concentration must have blocked the alumina hydroxyls.

The TPD spectra of CO adsorbed on the $Pd–20Mo/Al_2O_3$ catalyst (Fig. 3) were very similar to the desorption profile for the $20Mo/Al_2O_3$ catalyst. Although Pd was present, the CO and CO_2 yields were the same as those for the Mo-only catalyst (Table 4). This suggests that Pd may be partially covered due to the high Mo content on this catalyst. It is known that an MoO_3 monolayer on alumina is formed between an Mo loading of 8 to 12% (5, 21). In this case, the 20% Mo concentration should lead to the formation of bulk MoO_3, which may cover part of the Pd particles. To confirm this, CO and H_2 chemisorption measurements were performed with the three catalysts and the results may be seen in Table 3. Hydrogen adsorption on the Pd/Al_2O_3 catalyst is 3 times higher than that on the $Pd–20Mo/Al_2O_3$ catalyst and 7 to 8 times higher than that on the $20Mo/Al_2O_3$ catalyst. This leads one to believe that Pd particles are, in fact, partially covered by the molybdenum oxide. On the other hand, CO adsorption on Pd/Al_2O_3 is 10 times lower than that on $20Mo/Al_2O_3$ and 17 times lower than that on the $Pd–20Mo/Al_2O_3$ catalyst. Previous TPR results revealed that the presence of palladium strongly increased the amount of partially reduced molybdenum oxide species (7). TPR measurements were also made for the catalysts studied here (not shown) and the promotional effect of palladium on the reduction of molybdenum oxide was also observed. Hence, the difference in CO adsorption between the two Mo-containing catalysts is due to the larger amount of partially reduced molybdenum oxide in the $Pd–20Mo/Al_2O_3$ catalyst. This effect was also seen in the TPD results, in which the amounts of CO and CO_2 desorbed were greater with the $Pd–20Mo/Al_2O_3$ sample (Table 4).

NO Adsorption

The TPD spectra for NO adsorption on Pd/Al_2O_3 (Fig. 4) presented a great amount of unreacted NO desorbing at lower temperatures (42% yield, as seen in Table 4). NO decomposition only started above 600 K.

For the $20Mo/Al_2O_3$ catalyst (Fig. 5), all the NO initially adsorbed decomposed to form N_2 and N_2O as the main products. In this case, decomposition began around 450 K. TPD analysis of CO and NO adsorption on ceria-supported Pd catalysts (22) revealed that the presence of ceria significantly improved NO dissociation. Rao *et al.* (23) also reported evidence for NO dissociation on catalysts containing reduced ceria. According to Praliaud *et al.* (24), the reduction of NO on ZrO_2-supported Pd catalysts involves the oxygen vacancies created on the support. In a previous work, IR measurements have shown the presence of NO adsorption on partially reduced molybdenum oxide on the Mo/Al_2O_3 catalyst (8). In this study, DRIFTS analysis of NO on Mo/Al_2O_3 revealed a strong increase in the band intensity for adsorbed NO after reduction (Fig. 13). Thus, the enhancement of NO dissociation to N_2 and N_2O could be attributed to the presence of reduced molybdenum oxide, as proposed for CeO_2 and ZrO_2.

On the $Pd–20Mo/Al_2O_3$ catalyst, NO adsorption increased when compared to that on the other catalysts (Table 4). Once again, this may be explained by the greater amount of partially reduced molybdenum oxide in the Pd–$20Mo/Al_2O_3$ sample, since the presence of Pd promotes

the reduction of MoO_3 (4, 7). Furthermore, the N_2 yield was higher, showing a large and narrow peak at 560 K. This peak was not present on the $20Mo/Al_2O_3$ catalyst. Apparently, the second peak for N_2 formation (at 780 K) is the same for both catalysts. According to Vesecky *et al.* (25) and Noronha *et al.* (8), the high-temperature peak may be attributed to strongly bonded, inactive, adsorbed nitrogen species (N_a), which inhibit further NO adsorption and dissociation. The presence of partially reduced molybdenum oxide decreases the presence of such inactive species, thus favoring N_2 formation at lower temperatures. However, since N_2 formation on $Pd–20Mo/Al_2O_3$ began at temperatures 100 K higher than that on $20Mo/Al_2O_3$, it is possible that new adsorption sites at the palladium–molybdenum interface have been formed, which favor formation of the active nitrogen surface species. This proposal is consistent with the work of Noronha *et al.* (8). Hence, the presence of Pd together with molybdenum oxide in a high concentration promotes both NO adsorption and NO decomposition to N_2.

Adsorption of Ethanol

TPD results showed that alumina presented high selectivity toward dehydration of ethanol. This was also observed by McCabe and Mitchell (10), who attributed it to the presence of strong acid sites. Although Cordi and Falconer (13) observed the same effect, they also verified some dehydrogenation of ethanol to acetaldehyde and H_2. The IR analyses showed a decrease in the intensities of the bands related to ethoxy species when the temperature was raised. This indicates that some of the ethoxy species desorbed as ethanol and some dehydrated to form ethylene.

The addition of Pd led to the decomposition and the dehydrogenation of ethanol. A similar result was obtained by Cordi and Falconer (13) and they suggested that part of the ethanol adsorbed on alumina diffused to Pd sites to decompose. According to them, the α-carbon formed CO and the β-carbon formed CH_4 during ethanol decomposition. However, the amounts of CH_4, CO, and H_2 formed at low temperature were greater than those observed here. According to Nagal and Gonzalez (26), the catalytic oxidation of ethanol on Pt/SiO_2 occurs by a mechanism assuming dehydrogenation of an ethoxy intermediate as the rate-determining step. A monodentate surface acetate is formed during oxidation of the dehydrogenated species. This acetate intermediate may then react to form CO_2. On the other hand, the dehydrogenated species can also produce CO_2 and CH_4 by decomposition. Therefore, for the Pd/Al_2O_3 catalyst, part of the ethoxy species adsorbed on alumina probably migrates to the Pd sites where a fraction decomposes to form CO, CH_4, and H_2 and another fraction reacts to form acetate species, which are more stable and remain adsorbed until 573 K, as revealed by IR analysis (Fig. 12). These acetate species could be the precursors for the formation of CO and CO_2 at high temperature, as observed in the TPD experiments (Fig. 8). Above 723 K, the acetate species may decompose and/or react with surface hydroxyls of the support.

For the catalysts containing Mo, there was a drastic reduction of ethylene formation. This reaction is mainly catalyzed by the acid sites on alumina; however, since the MoO_3 concentration is high, most of the alumina acid sites must have been blocked by formation of monolayer. Another feature presented by the 20Mo and Pd–20Mo catalysts was the presence of two peaks for acetaldehyde (Figs. 9 and 10). Iwasawa *et al.* (27) studied the reaction intermediates in ethanol oxidation over silica-supported molybdenum oxide catalysts by using IR spectroscopy. The bands observed were attributed to the ethoxide structure. *In situ* Raman spectroscopy under the reaction conditions identified two types of ethoxide species which were associated with Mo=O and Mo–O–Mo sites (28). The ethoxide species bonded to a terminal oxygen group produced acetaldehyde, while the ethoxide species bonded to a bridging oxygen group produced ethylene. In addition, they suggested that the reactivity for ethanol oxidation over MoO_3 dispersed on SiO_2, Al_2O_3, and TiO_2 was associated with the reducibility of the surface molybdate. Therefore, the first acetaldehyde peak was present only on the catalysts containing molybdenum oxide and could be attributed to the dehydrogenation of ethanol adsorbed on partially reduced molybdenum oxide. The second was observed on palladium- and molybdenum-based catalysts. It was probably due to the dehydrogenation of the ethoxy species initially adsorbed on alumina, which migrate to the active sites (MoO_x in the case of 20Mo catalyst and MoO_x and Pd^o in the case of Pd–20Mo catalyst).

In spite of the presence of Pd, the $Pd–20Mo/Al_2O_3$ catalyst did not show high selectivity for the decomposition of ethanol to CO, CH_4, and H_2 at low temperatures. In fact, the TPD profile for the $Pd–20Mo/Al_2O_3$ catalyst was very similar to the TPD profile for the $20Mo/Al_2O_3$ catalyst. This behavior is similar to the TPD of CO adsorbed on these catalysts. Once again, this may be attributed to the presence of bulk MoO_3 (due to the high Mo loading) that partially covers the Pd metallic sites, making it appear as if the presence of Pd had no direct effect on the properties of the 20Mo catalyst for the adsorption of ethanol. Furthermore, since the presence of Pd favors the reduction of MoO_3 (4, 7), it seems that the amount of partially reduced molybdenum oxide has a smaller effect on ethanol adsorption than on NO adsorption. Although the intensities were weaker, when compared to the TPD results for Pd/Al_2O_3, the Mo-containing catalysts also showed desorption of CO, CO_2, and H_2 at higher temperatures. Once again, this might be due to the decomposition and/or reaction of a carbonaceous species that remained adsorbed with surface hydroxyls on the alumina.

CO + NO Reaction and DRIFTS Measurements

Figure 14b displays the peaks resulting from the NO + CO reaction on the Pd–20Mo/Al_2O_3 catalyst at 573 K in the DRIFTS cell, compared to the Pd/Al_2O_3 (Fig. 14a) catalyst. Pd^+–NO species are around 1590 cm^{-1}. The Pd–Mo/Al_2O_3 catalyst exhibited new bands with quite different intensities as the NO–Mo bands occur at 1800 and 1700 cm^{-1}. The band at 1566 cm^{-1} is attributed to NO_2 formation. The adsorbed NO_2 species were formed after reaction of adsorbed NO with the oxygen bonded to Pd, which was created by the dissociation of NO. In addition, the band in the neighborhood of 2258 cm^{-1} corresponds to an isocyanate complex (7, 29) produced according to the following reaction:

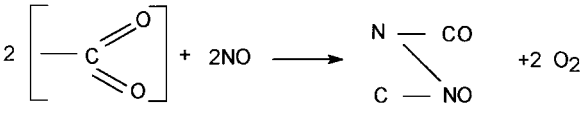

In a previous study (7) of a Pd–8% Mo/Al_2O_3 catalyst, it was shown that the CO + NO reaction was promoted by the presence of partially reduced molybdenum oxide in contact with Pd particles. An oxidation–reduction mechanism was proposed in which NO molecules react with MoO_x sites to give N_2 and supply oxygen to react with Pd–CO_{ads} species. Furthermore, the adsorption of CO molecules on the Mo surface acts as a supply of CO to Pd particles surrounded by Mo. The larger the amount of Mo surrounding the Pd particles, the larger the promotion capability of these Mo species.

In this work, the 20% Mo loading would assure an intimate contact between Pd and Mo. The rate of NO conversion and the selectivity for N_2 formation, as a function of temperature for both catalysts in the reducing condition, may be seen in Fig. 15. Between 473 and 593 K the rate over Pd–20Mo/Al_2O_3 was higher than that over Pd/Al_2O_3. The selectivity to N_2 at lower temperatures was initially very high (ca. 100% at 473 K), but decreased with increasing temperature up to 573 K and then remained constant. The only other product besides CO_2 and water was N_2O.

The selectivity between N_2 and N_2O was obtained for low conversion at 493 K, as displayed in Table 5. The addition of MoO_3 improved the selectivity for N_2. Similar results were obtained by Gandhi *et al.* (4) and Halasz *et al.* (5). According the latter authors, the high $N_2 + N_2O$ selectivity is due to the molybdena contribution to the high-temperature catalytic properties of the Pd–20Mo/Al_2O_3 under oxygen-free conditions (5). Therefore, even though Pd particles may be partially covered, as discussed before, the intimate contact between Pd and Mo obtained from the high Mo concentration assured the promotional effect caused by molybdenum. This may be explained by the mechanistic aspects of the reaction. It is not necessary for palladium particles to be close to each other, since NO is reduced by MoO_x and the oxygen is transferred to palladium which oxidizes adsorbed CO. Therefore, it is important for Pd to be in good contact with Mo. This interaction between Pd–Mo on Pd–20Mo/Al_2O_3 catalyst is enough to account for the fact that Pd particles are partially covered by Mo.

Nevertheless, the DRIFTS spectra indicated that NO forms isocyanate species, as mentioned before. These species can also be an intermediate and contribute to NO_x reduction. However, the DRIFTS spectra (Fig. 14) show that the isocyanate species in the neighborhood of 2258 cm^{-1} are present on both catalysts (Pd/Al_2O_3 and Pd–20Mo/Al_2O_3) with the same intensity. This result would not explain the higher activity of the Pd–20Mo/Al_2O_3 catalyst. Therefore, it seems that this reaction pathway is not favored for the CO + NO reaction. Instead, the oxidation–reduction mechanism seems to be more important.

In fact, when an oxidizing condition was used for this reaction on Pd–20Mo/Al_2O_3 catalyst, the activity dropped (Fig. 16). This suggests that the oxidizing atmosphere may have diminished the amount of reduced Mo, hampering the reaction. However, the selectivity for N_2 was not significantly changed, indicating that the reaction mechanism (redox mechanism) was not affected.

On the Pd/Al_2O_3 catalyst, the effect of the oxidizing condition was completely the opposite, since no redox mechanism happens (the reaction occurs on the palladium metallic surface). Instead, the larger amount of NO molecules (excess NO on the reaction feed) leads to an increase in the activity (Fig. 16).

Ethanol + NO Reaction

The NO + ethanol reaction on the Pd/Al_2O_3 catalyst showed enhanced activity for the conversion of NO when compared to the Pd–20Mo/Al_2O_3 catalyst for either reducing or oxidative conditions. Unlike the CO + NO reaction, it seems that for NO reduction by ethanol it is important that Pd particles are exposed. Indeed, TPD of adsorbed ethanol revealed that the Pd coverage by MoO_x decreased the ethanol decomposition; however, the amount of reduced molybdenum oxide had no effect on ethanol adsorption. Furthermore, molybdenum oxide does not promote the ethanol + NO reaction as it does for the CO + NO reaction and this may be due to different reaction mechanisms. It seems that for the NO + ethanol reaction the oxidation–reduction mechanism proposed for the CO + NO reaction is not the main reaction pathway. In a previous work (31) TPSR measurements of NO + ethanol on Pd–Mo catalysts showed that the presence of NO hampered the ethanol decomposition on Pd sites and the reaction between ethanol and NO took place only above 573 K. Below this temperature, ethanol only decomposed on the support. For the reaction studied here, Tables 6 and 7 show that ethanol conversion is much higher than would be expected for the total reduction of NO and total oxidation of ethanol, as

shown below:

$$6NO + CH_3CH_2OH \rightarrow 3N_2 + 2CO_2 + 3H_2O. \quad [3]$$

Moreover, no significant formation of acetaldehyde and CO is observed, which are products of ethanol decomposition on the Pd surface as observed from TPD results on Pd/Al_2O_3 catalyst (Fig. 8). This indicates that part of the ethanol must be decomposing on the support. In fact, Tables 6 and 7 show that for the Pd/Al_2O_3 catalyst there is a high selectivity for ethylene, which is the main decomposition product of ethanol on alumina, as seen on TPD of adsorbed ethanol (Fig. 7). Furthermore, the formation of ethylene during TPD is between 500 and 600 K, which is exactly the temperature range studied here.

Another interesting point is that when the reaction condition is changed from reducing to oxidative, the decomposition reaction of ethanol on alumina significantly decreased as temperature was raised. In Table 6, the ethylene selectivity began at 62% (553 K) and then remained around 45% (573 and 593 K). On the other hand, Table 7 shows that the selectivity for ethylene began at 95% (523 K) and decreased to 6% (593 K), while the selectivity for CO_2 increased. This may be due to the relative amounts of NO and ethanol in the different feeds. Under the reducing condition there is excess of ethanol and therefore it is more likely to have enough ethanol to decompose on the alumina surface even when the temperature is raised and the NO + ethanol reaction on Pd particles increases. On the other hand, under the oxidative condition there is an excess of NO. Hence, as the temperature is raised, so is the NO + ethanol reaction on the Pd sites and less ethanol is available to decompose on alumina.

A similar result is observed for the $Pd–20Mo/Al_2O_3$ catalyst. However, the high Mo loading covers a great part of the alumina surface and therefore the selectivity for ethylene is very low. Nevertheless, acetaldehyde is formed, since it is an important decomposition product of ethanol on partially reduced molybdenum oxide, as observed from TPD results (Figs. 9 and 10). Noteworthy is that for this catalyst, the activity for NO reduction decreased under the oxidative condition, since the oxidizing atmosphere may have diminished the amount of reduced Mo.

CONCLUSION

The presence of partially reduced molybdenum oxide improved the NO dissociation to N_2 on a Pd–Mo catalyst. The $Pd–20Mo/Al_2O_3$ catalyst showed better activity and selectivity for N_2 formation during the CO + NO reaction. Both TPD of adsorbed CO and DRIFT spectra suggest that the reaction follows a redox mechanism. On the other hand, MoO_3 addition to a Pd/Al_2O_3 catalyst favored the formation of acetaldehyde at lower temperatures during TPD of adsorbed ethanol. It seems that the presence of molybdenum oxide partially covered the Pd particles, as evidenced by the absence of ethanol decomposition products during TPD of adsorbed ethanol and also by the lower activity of the $Pd–20Mo/Al_2O_3$ catalyst for the ethanol + NO reaction compared to Pd/Al_2O_3. For the NO reduction by ethanol it is important that Pd particles are exposed. Molybdenum oxide does not promote the ethanol + NO reaction as it does for the CO + NO reaction and this may be due to different reaction mechanisms. The selectivity distribution for the NO + ethanol reaction suggest that the decomposition of ethanol on the support seems to be an important side reaction on the Pd/Al_2O_3 catalyst. However, the molybdenum oxide addition decreased this reaction due to alumina coverage.

ACKNOWLEDGMENTS

To CAPES for the scholarship (L.F.M.), to Penn State University, CNPq, NSF (M.S), and PRONEX for financial support.

REFERENCES

1. Guerrieri, D. A., Caffrey, P. J., and Rao, V., *SAE Paper 950777* (1995).
2. Altshuller, A. P., *Atmos. Environ. A* **27**, 21 (1993).
3. Miguel, A. H., and Andrade, J. B., *J. Bras. Chem. Soc.* **1**, 124 (1990).
4. Ghandi, H. S., Yao, H. C., and Stepien, H. K., *in* "Catalysis Under Transient Conditions" (A. T. Bell and L. L. Hegedus, Eds.), ACS Symposium Series 178, p. 143. Am. Chem. Soc., Washington, DC, 1982.
5. Halasz, I., Brenner, A., Shelef, M., and Ng, S., *Appl. Catal. A: Gen.* **82**, 51 (1992).
6. Halasz, I., Brenner, A., and Shelef, M., *Appl. Catal. B: Environ.* **2**, 131 (1993).
7. Schmal, M., Baldanza, M. A. S., and Vannice, M. A., *J. Catal.* **185**, 138 (1999).
8. Noronha, F. B., Baldanza, M. A. S., and Schmal, M., *J. Catal.* **188**, 270 (1999).
9. Yao, Y. Y., *Ind. Eng. Chem. Process Des. Dev.* **23**, 60 (1984).
10. McCabe, R. W., and Mitchell, P. J., *Ind. Eng. Chem. Prod. Catal. Dev.* **23**, 196 (1984).
11. Rajesh, H., and Ozkan, U. S., *Ind. Eng. Chem. Res.* **32**, 1622 (1993).
12. Mao, C., and Vannice, M. A., *J. Catal.* **154**, 230 (1995).
13. Cordi, E. M., and Falconer, J. L., *J. Catal.* **162**, 104 (1996).
14. Idriss, H., Diagne, C., Hindermann, J. P., Kiennemann, A., and Barteau, M. A., *J. Catal.* **155**, 219 (1995).
15. Bollinger, M. A., and Vannice, M. A., *Appl. Catal. B: Environ.* **8**, 417 (1996).
16. Greenler, R. G., *J. Chem. Soc.* **82**, 2488 (1962).
17. Rieck, J. S., and Bell, A. T., *J. Catal.* **96**, 88 (1985).
18. Rieck, J. S., and Bell, A. T., *J. Catal.* **99**, 262 (1986).
19. Rieck, J. S., and Bell, A. T., *J. Catal.* **103**, 46 (1987).
20. Hoost, T. E., Otto, K., and Laframboise, K. A., *J. Catal.* **155**, 303 (1995).
21. Portela, L., Grange, P., and Delmon, B., *Catal. Ver. Sci. Eng.* **37**(4), 699 (1995).
22. Cordatos, H., and Gorte, R. J., *J. Catal.* **159**, 112 (1996).
23. Rao, G. R., Fornasiero, P., Di Monte, R., Kaspar, J., Vlaic, G., Balducci, G., Meriani, S., Gubitosa, G., Cremona, A., and Graziani, M., *J. Catal.* **162**, 1 (1996).
24. Praliaud, H., Lemaire, H., Massardier, A., Prigent, J., and Mabilon, G., *in* "Proceedings, 11th International Congress on Catalysis, Baltimore,

1996" (J. W. Hightower, W. N. Delgass, E. Iglesia, and A. T. Bell, Eds.), Vol. 101, p. 345. Elsevier, Amsterdam, 1996.
25. Vesecky, S. M., Rainer, D. R., and Goodman, D. W., *J. Vac. Sci. Technol. A* **14**, 1457 (1996).
26. Nagal, M., and Gonzalez, R. D., *Ind. Eng. Chem. Prod. Res. Dev.* **24**, 525 (1985).
27. Iwasawa, Y., Nakano, Y., and Ogasawara, S., *J. Chem. Soc. Faraday Trans.* **74**, 2986 (1978).
28. Zhang, W., Desikan, A., and Oyama, S. T., *J. Phys. Chem.* **99**, 14478 (1995).
29. Dompelmann, R., Cant, N. W., and Trimm, D. L., *Appl. Catal. B: Environ.* **8**, L219 (1995).
30. Ukisu, Y., Miyadera, T., Abe, A., and Yoshida, K., *Catal. Lett.* **37**, 265 (1996).
31. de Mello, L. F., Baldanza, M. A. S., Noronha, F. B., and Schmal, M., *Stud. Surf. Sci. Catal.*, in press.